ABSTRACT

Characterization of Aluminum Powder Ignition

by

Salil Mohan

Heating rate effect and particle size effect on ignition temperature of Al powder were studied to collect data for development of a possible Al powder ignition model. Aluminum ignition is associated with a highly accelerated burn rate and high combustion enthalpy. A new ignition model, which can adequately interpret these conditions, is needed to develop better propulsion fuels, explosives and incendiaries that use Al as an additive. This experimental program was focused on preparing framework for characterization of ignition kinetics of Al powder by determining the ignition temperature for different, systematically varied, heating rates and particle size. The experimental setup involved igniting Al powder; coated on a small length of an electrically heated carbon filament. A three-color pyrometer and a high-speed camera were used in the project to determine the filament surface temperature at the instant of ignition. When using the pyrometer, a sharp rise in a photodiode signal from the powder coating was used to determine the ignition moment. The high-speed camera recorded both the temperature and the ignition moment. Two Al powders with different particle size (Alfa Aesar, Al 10 – 14 μm and Al 3 – 4.5 μm) were investigated. The powders were ignited at three different heating rates. A higher ignition temperature was observed for higher heating rate for both the powders. The powder with larger particles ignited at higher temperature for same heating rate.

CHARACTERIZATION OF ALUMINUM POWDER IGNITION

by
Salil Mohan

A Dissertation
Submitted to the Faculty of
New Jersey Institute of Technology
In Partial Fulfillment of the Requirements for the
Degree of Master of Science in Mechanical Engineering

Department of Mechanical Engineering

January 2004

Approval Page

CHARACTERIZATION OF ALUMINUM POWDER IGNITION

Salil Mohan

Dr. Edward L. Dreizin, Thesis Advisor — Date
Associate Professor of Mechanical Engineering, NJIT

Dr. Chao Zhu, Committee Member — Date
Associate Professor of Mechanical Engineering, NJIT

Dr. Boris Khusid, Committee Member — Date
Associate Professor of Mechanical Engineering, NJIT

BIOGRAPHICAL SKETCH

Author: Salil Mohan

Degree: Master of Science

Date: January 2004

Undergraduate and Graduate Education:

- Master of Science in Mechanical Engineering,
  New Jersey Institute of Technology, Newark, NJ, 2004

- Bachelor of Technology in Mechanical Engineering,
  G.B.Pant University of Agricuture. And Technology; Pantnagar; India; 1997.

Major: Mechanical Engineering

Presentations and Publications:

Salil Mohan, M. A. Trunov, and E. L. Dreizin
"Characterization of Aluminum Powder Ignition,"
Eastern States Section of Combustion Institute Technical Meeting,
Penn State University, State College, Pennsylvania, October 2003.

To my beloved family

ACKNOWLEDGMENT

I would like to express my deepest thanks to Dr. Edward Dreizin, who was not only my research supervisor; but was a great source of motivation and encouragement; always providing his experience; insight and intuition. Special thanks are given to Dr. Boris Khusid and Dr. Chao Zhu for actively participating in my committee.

Many of my fellow graduate students in the Energetic Materials Research Laboratory are deserving of recognition for their support. I also wish to thank Mr. Michael A. Trunov for his constant assistance and guidance.

TABLE OF CONTENTS

TABLE OF CONTENTS
(Continued)

TABLE OF CONTENTS
(Continued)

LIST OF TABLES

LIST OF FIGURES

LIST OF FIGURES
(Continued)

Figure **Page**

LIST OF FIGURES
(Continued)

CHAPTER 1

INTRODUCTION

1.1 Background

Aluminum is a promising ingredient for high energy density fuels, which are used in variety of propulsion systems, explosives and pyrotechnics. It is widely used as an additive in such fuels to achieve high combustion enthalpy. The process of metal combustion occurs in environment with rapidly changing temperature and gas composition. Accurate models for metal ignition, that take into account these changes are needed for design and development of new propulsion systems and other applications utilizing metal combustion. The existing ignition models are inadequate in describing metal ignition as they fail to interpret the accelerated burn rates and high combustion enthalpies, characteristic of metal ignition. The current models [1 - 11] introduce critical environment temperature, T_{env}, and predict ignition when the particle is exposed to temperatures exceeding T_{env}. This approach is successful for applications with steady environment temperature i.e. for fire safety related ignition modeling. For applications of advanced energetic, that deal with rapidly changing temperature, ignition thermal kinetics must be taken into account.

Efforts to characterize aluminum ignition till now have produced inconsistent and contradictory results. Figure 1.1 plots the published data on aluminum particle size and ignition temperature. Temperatures as low as 850 K and as high as 2300 K have been reported as aluminum ignition temperatures by

different authors [1-11]. The reported ignition temperature appears to correlate with the sample size [12]. The discrepancies between the points reported by different authors may be attributed to different experimental methods employed, which resulted in different conditions, such as heating rates and surrounding gas compositions. Also, different definitions of ignition moment used by different authors could have led to variations in the reported values of ignition temperatures.

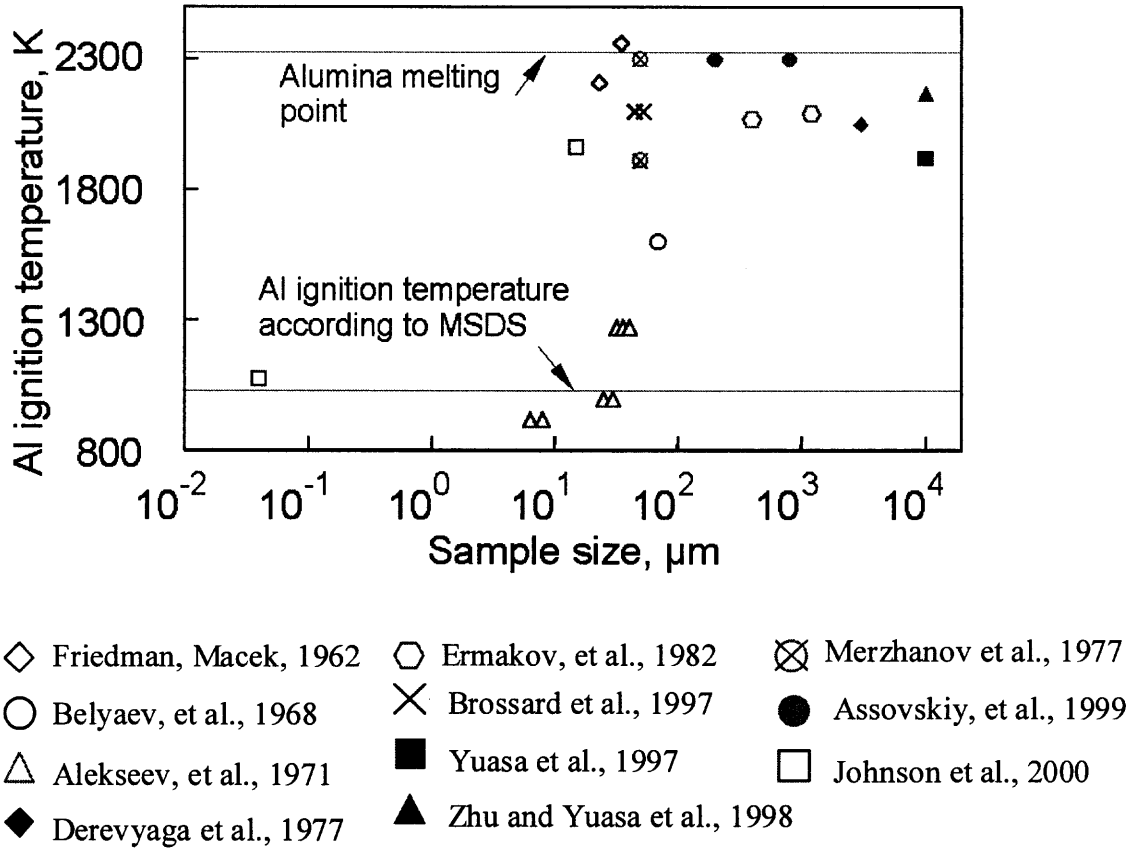

Figure 1.1 Summary of experimental results on aluminum ignition, [1-11].

1.2 Objective

The presented work is aimed to develop an experimental approach to characterize ignition of metallic fuel powder. The specific objective was to collect experimental data on ignition temperature of aluminum powder as a function of heating rate and particle size, which can be utilized to obtain preliminary information on thermal kinetics. The collected experimental data can further be used to develop a model for Al ignition, which can predict ignition of Al for different practical applications.

CHAPTER 2

EXPERIMENTAL SETUPS AND TECHNIQUES

2.1 General Description

The experiments were performed with a thin layer of the powder under investigation, placed on a short portion (~ 5 mm) of an electrically heated carbon filament (Alfa Aesar, carbon yarn woven from 0.076mm dia. fibers, 99.96% metal basis). The filament heats the powder, igniting it at a certain temperature. Figure 2.1 shows a schematic diagram of a fixture used for holding the filament. The filament is held in place by screw clamps on two metallic brackets. One bracket is mounted on a linear slide and the other is fixed. The sliding bracket allows clamping different lengths of filament. The metallic brackets are connected to D.C. power source (D.C. 4 x 12 V, WestCo Battery Inc.), used to heat the filament.

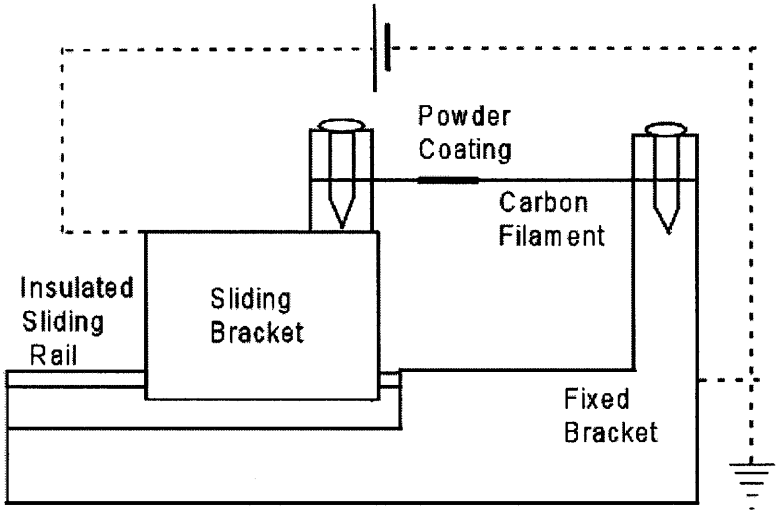

Figure 2.1 Filament mounting setup.

The objective of the experiment is to identify the ignition instant and ignition temperature. The ignition temperature is defined in the study as the temperature of heated filament at the ignition instant. In the first approximation, the temperature of fine particles forming the coating on the filament could be assumed to follow the filament temperature exactly. In the future work, a more accurate model will be developed that would correlate the temperature of igniting particles with the measured filament temperature.

Two techniques were used to determine the ignition moment and ignition temperature. One technique (see Figure 2.2a) utilized a three-color pyrometer (500nm, 568 nm and 610 nm) and a photodiode; the other (see Figure 2.2b) used a high-speed video camera (PCI based MotionPro500 high-speed CMOS imaging system). Both techniques use the same approach for the filament heating and powder ignition, the difference is in the equipment used for identification of the ignition instant and temperature. The pyrometer technique uses a three-color optical pyrometer to measure the filament surface temperature and a photodiode, focused on the powder coating, determines the ignition instant. The camera technique, on the other hand, uses only a high-speed camera. The camera films the powder coating as well as the adjacent filament surface. Thus, the ignition instant and the filament surface temperature were obtained from the analysis of the same film frame sequence.

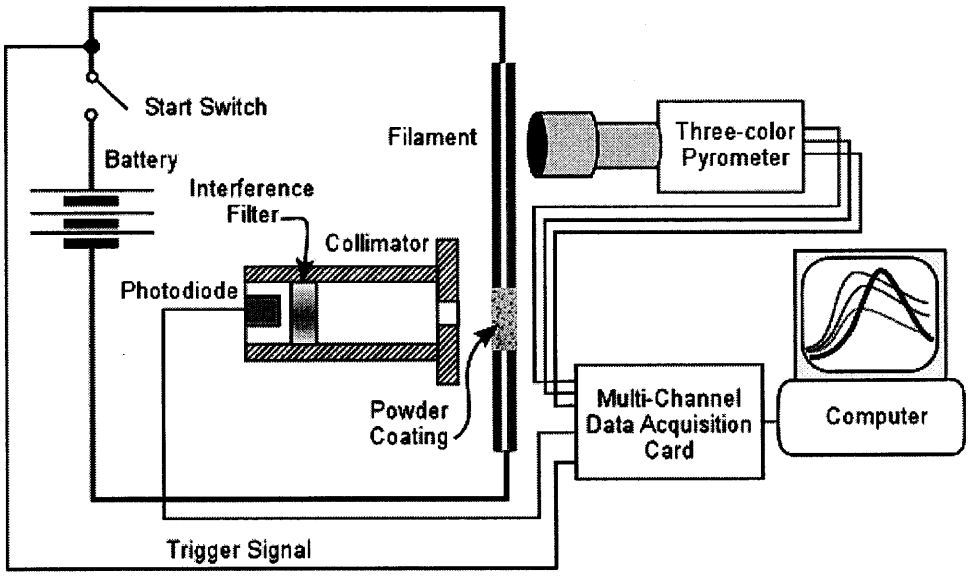

Figure 2.2a Experimental setup of the pyrometer and photodiode temperature-measuring technique.

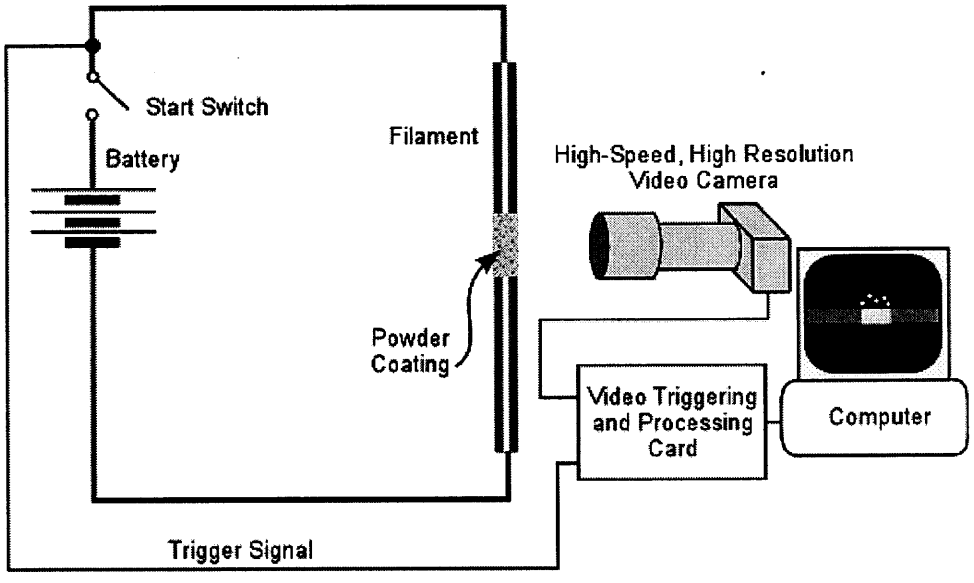

Figure 2.2b Experimental setup of the high-speed camera temperature-measuring technique.

2.2 Investigated Material

Two different particle size, 3-4.5 μm and 10 – 14 μm, of aluminum powder (Alfa Aesar) were investigated for ignition temperature and heating rate dependence. Figure 2.3a shows the SEM (Scanning Electron Microscopy, LEO 1530 FE-SEM) images and Figure 2.3b shows the particle size distributions of the investigated powder measured, using Low Angle Laser Light Scattering (Coulter-LS-230 particle size analyzer).

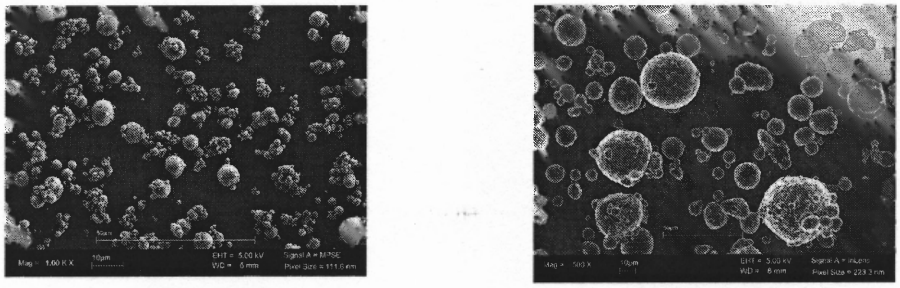

Al 3 – 4.5 μm **Al 10 – 14 μm**

Figure 2.3a SEM images of Al 3-4.5 μm and Al 10 – 14 μm.

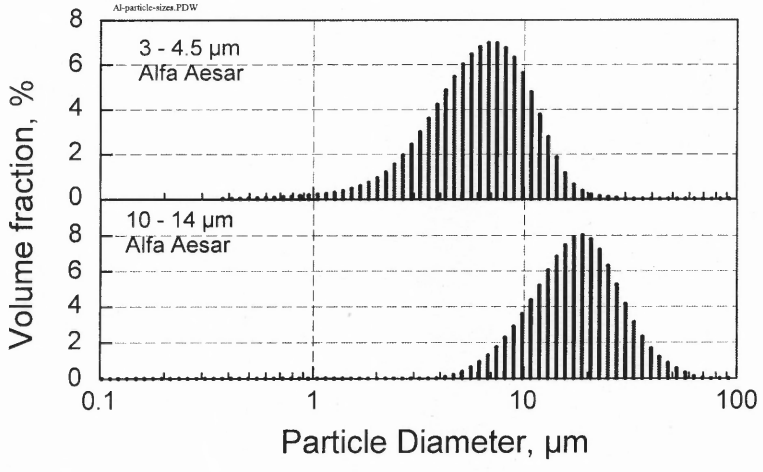

Figure 2.3b Particle size distributions of investigated powders.

2.3 Experimental Run Preparations

2.3.1 Filament Clamping

A segment of approximately 6 – 7 cm of the carbon filament length is cut and fixed using screw clamps on any of the two brackets – Figure 2.1. After that, the filament is twisted 7 – 10 turns around its axis and its twisted end is attached to the second bracket. The filament was repeatedly twisted to achieve better a reproducibility of the filament diameter. Finally, the filament is straightened out by gently pulling back the sliding bracket. In most experiments, the distance between the brackets was set at 53 $\pm$ 1 mm. In some tests, this distance was set at 30 mm to achieve a high heating rate.

2.3.2 Powder Coating Preparations

To prepare a thin coating on the filament, a small paintbrush (3mm wide) is used. A small amount of the investigated powder is placed on the glass slide. The paintbrush is wet in water and used to make a dense powder suspension on the glass slide. The brush is then used to make a thin coating, approximately 5 mm wide, in the middle of the filament. The coating is left to dry at room temperature for 30 minutes. It was observed that during that time, the thick unused powder suspension left on the slide and the paintbrush dried, therefore we were certain that the powder coating on the filament dried as well. After drying the coating was ready for an ignition test.

2.3.3 Heating Rate Control

Different heating rates were obtained using different DC power sources used for filament heating. Three different heating rates were used by employing 24 V, 36 V and 48 V DC power source with 53 $\pm$ 1 mm of filament length. Use of higher voltage power source gave higher heating rates. A combination of the 48 V DC power source with the 3 cm filament length was used to achieve the highest heating rate employed in this project.

2.4 Three Color Pyrometer and Photodiode Technique

2.4.1 Experimental Setup & Procedures

Pyrometer and Photodiode Focusing:

The photodiode is focused on the powder coating so that it collects radiation only from the powder and not from the adjacent filament surface. The pyrometer, on the other hand, is focused on the filament surface area located about 10 mm afar from the powder coating. The field of view of the pyrometer includes about 2-5 mm of the filament length. For restricting the area of signal collection by the pyrometer and photodiode, slits made of blade edges were used, Figure 2.4. The slits were just wide enough (around 1 mm) to produce an optical signal of sufficient intensity to be registered by photodiode and pyrometer, respectively. The surfaces of the blade edge slit were painted black to avoid any reflection.

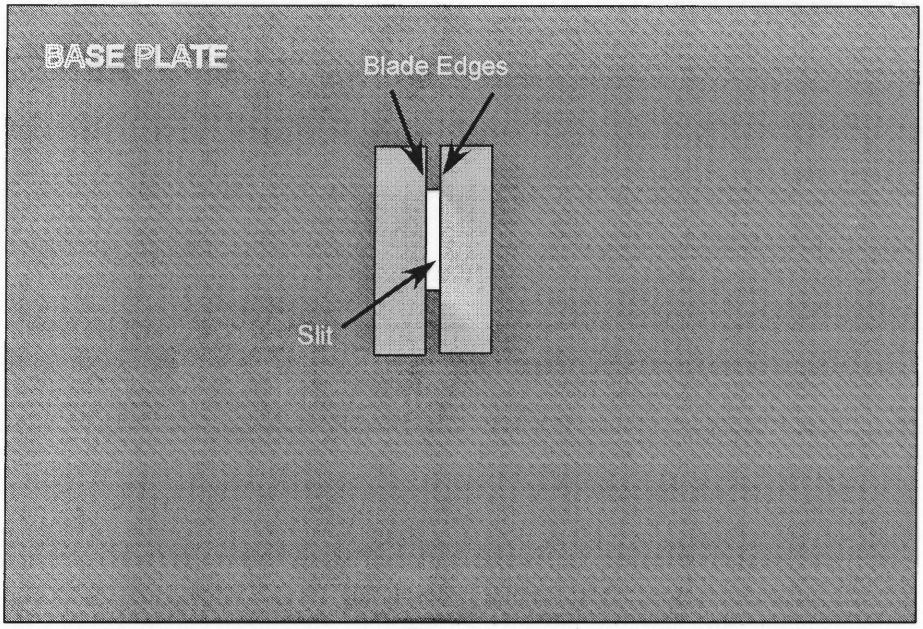

Figure 2.4 Design of Blade Edge Slits.

Data Acquisition Board triggering and Data Socket Board channels utilization:

A National Instruments data acquisition system was used to record data in this project. It consisted of a DAQ card (PCI-MIO-16E-4) installed in a desktop computer (Dell Dimension L866r). The DAQ card is connected to a data acquisition socket board (National Instrument, BNC2100, Figure 2.5), a hub for all recorded signals (coaxial cables) from the experimental setup. The DAQ card allowed simultaneous recording of eight channels, which corresponds to eight I/O terminals (ACH0...ACH7) on the data acquisition socket board. Figure 2.5 shows the layout of terminals on the data acquisition socket board. All terminals are identified by the names on the board (i.e. ACH 0,1,2...). The I/O terminals (ACH) have option for floating (FS) or grounded (GS) signal acquisition. All experiments

were recorded in the floating acquisition mode. Terminal PFI 0 is for an external triggering signal. The data acquisition card was triggered externally using analog signal from a resistive voltage divider connected across the filament, Figure 2.6. Seven terminals were used to record the experimental data. Because the analog triggering was utilized, the terminal ACH 0 was not used for recording, following manufacturer instructions. Terminals ACH1, ACH2 and ACH3 were used to record the three-color pyrometer data. Terminal ACH5 was used to measure the photodiode signal. The terminal ACH4, preceding the photodiode terminal, was short-circuited and recorded to reduce the channel interference effect (due to a high impedance of the photodiode circuit). No other signal showed the signal interference. Moreover, as a useful practice, the data recording terminals that were not in use were short-circuited to eliminate possible charge build-up and interference with other channels. In the present case, all channels were in use except ACH0, which was short-circuited. Terminals ACH6 and ACH7 were used for recording the current through the filament and the voltage across the filament, respectively.

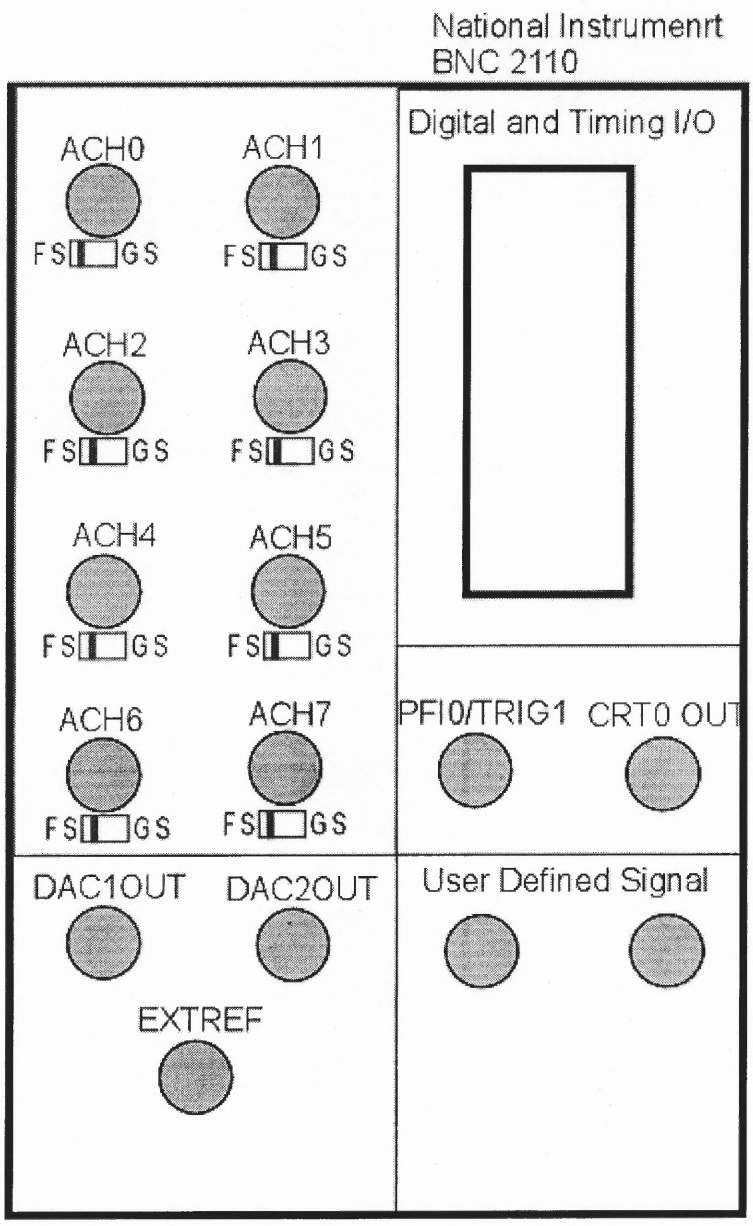

Figure 2.5 Data Acquisition Socket Board (National Instrument, BNC 2110).

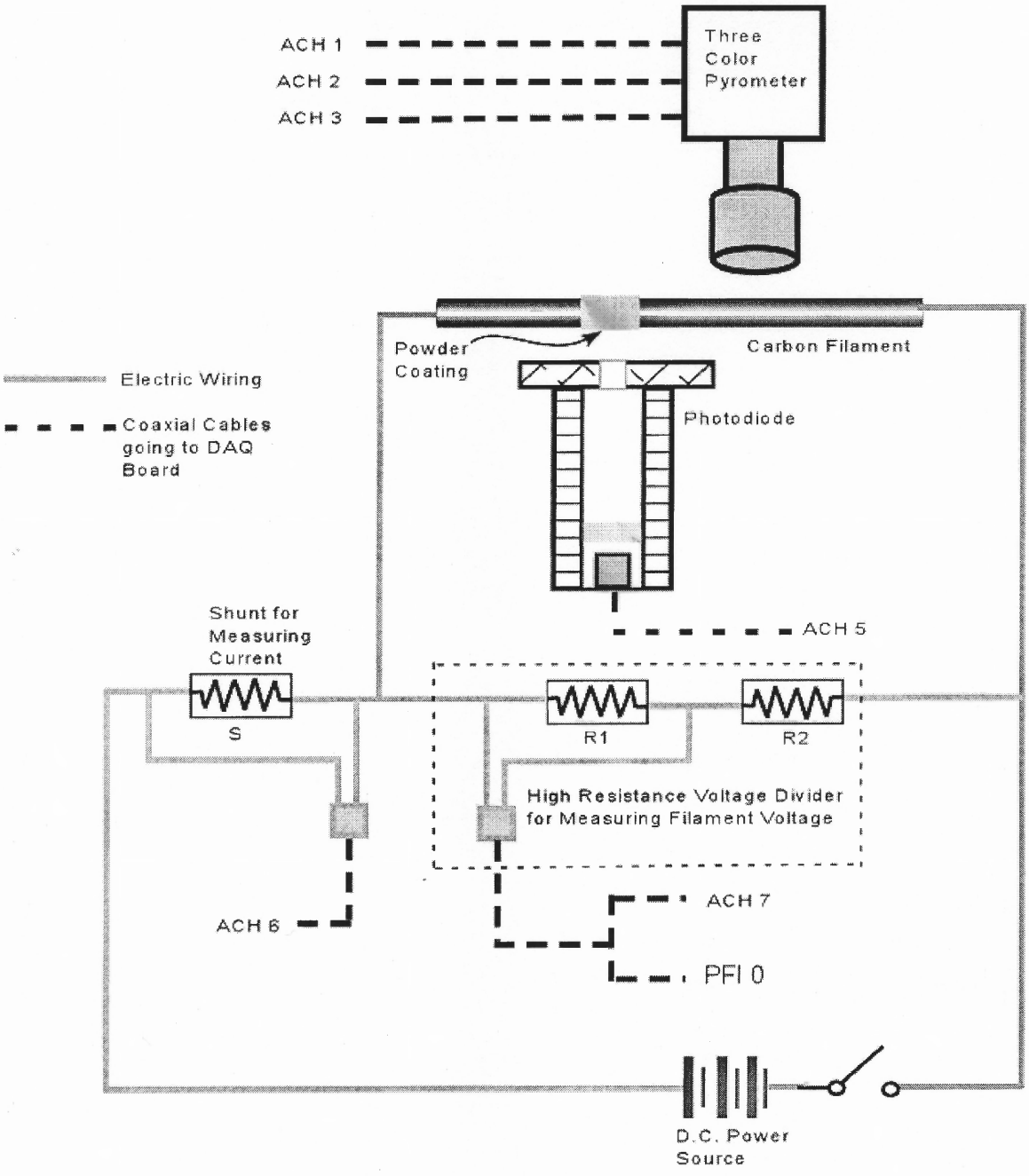

Figure 2.6 Experimental setup and electrical connections for pyrometer and photodiode technique.

2.4.2 Data Collection and Processing

Templates for Data Collection:

The DAQ card collected signals from seven channels at 10,000 scan per second (sps). The data are saved in an excel file. Measurements from each channel correspond to a separate column in the file. A MS excel macro is then developed that deletes the column in which data from the short-circuited channel (ACH4) were recorded. After that, the macro reduces the 10,000 sps data to 1000 sps data by converting the data series consisting of ten data points to a single point using a simple average. This reduced 1000 sps data set is used in the developed processing template

Signal Averaging:

The template uses an eleven point sliding average of the pyrometer channel data to calculate the experimental temperature. The eleven point sliding average implies that the value of the signal at any point in time, t_n, is the average of the data obtained at the instant of t_{n-5} to t_{n+5}.

$$(t_n)_{average} = \frac{t_{n-5} + t_{n-4} + \ldots\ldots + t_n + \ldots\ldots + t_{n+4} + t_{n+5}}{11}$$

Thus, the sliding average processed data recorded over 11ms.The averaging was used to reduce the high level of noise in the raw pyrometer data.

Determination of Ignition Moment:

The pyrometer technique uses the signal from the photodiode, which is focused on the powder coating surface area, to identify the ignition instant. A sharp increase in the photodiode signal would be an indicator of ignition. However, for the carbon filament, the temperature dependent electrical resistance affected the

increase in the radiation signal. For graphite, this dependence is shown in Figure 2.7 [13]. The effect of this dependence is that the diode signal (photodiode focused on the powder) shows a sharp rise due to an increased filament temperature, in addition to a sharp rise due to powder ignition. To analyze the interference of the two processes causing sharp rise in the photodiode signal, we compared the photodiode signal with one of the pyrometer channels signal (thus the pyrometer serving as second photodiode focused on filament surface). Moreover, we performed a separate experiment in which powder coating was not applied and photodiode was focused on the uncoated filament surface, for further comparision.

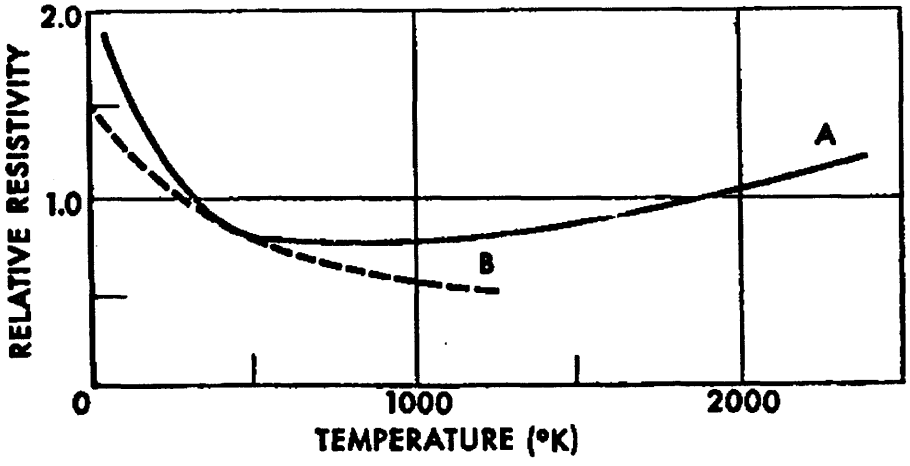

Figure 2.7 Electrical resistivity versus temperature for coke base (A) and lamp (B) base graphite [13].

Examples of the recorded signals without and with the powder coating are shown in Figure 2.8. To interpret the signals better we compared the derivatives of the photodiode and pyrometer channel signals. Figure 2.8a compares the

recorded signals and their derivatives for photodiode and pyrometer channel signals obtained in the experiments without powder coating. The photodiode and pyrometer are both looking at the filament surface but at slightly offset locations. The derivatives of both signals are following each other closely. Figure 2.8b represents the case when powder was placed on the filament. For this case, the derivative comparison shows a second peak only on the photodiode curve, which is attributed as powder coating ignition. The comparison of derivatives allowed an accurate identification of the instant of a fast increase in the photodiode signal (when the photodiode was focused on the powder) while the pyrometer signal showed the raise with a nearly constant rate. This instant was interpreted as the ignition of the powder coating.

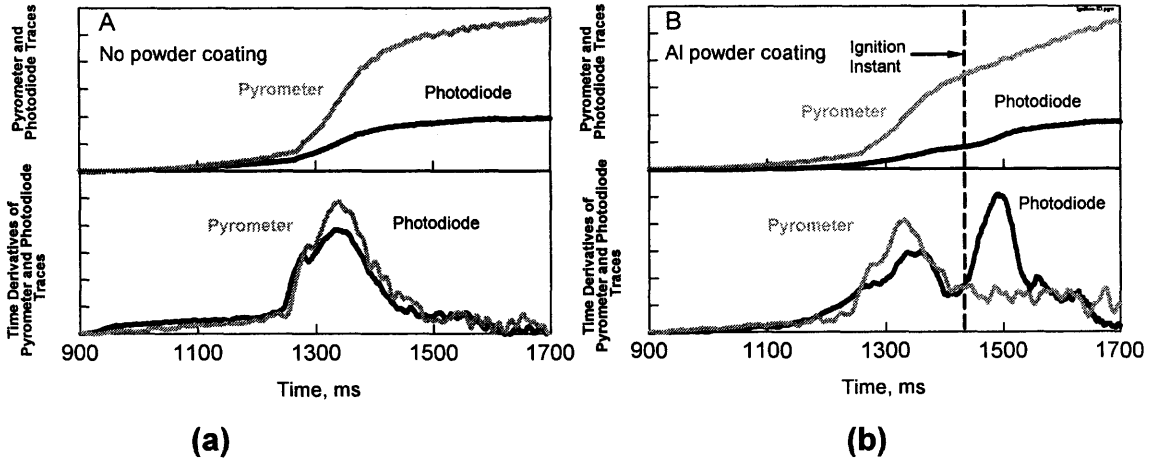

Figure 2.8 Comparison of photodiode and a pyrometer channel signal.
Top: Original Signals. Bottom: Derivatives.(a) Without powder on the filament (both pyrometer & photodiode focused on filament), (b) With powder coating (Pyrometer focused on filament & photodiode on powder).
Heating Rate is about 3000 K/s.

At high heating rates, the analysis of signal's derivatives was more complicated due to the nearly complete overlap of the photodiode derivative peaks related to the acceleration of the filament temperature and to the powder ignition. Figure 2.9 shows an example of signals measured at a higher heating rate (about 15000 k/s). The peaks on the photodiode curve are overlapped so much that the ignition peak is not distinguishable. However, the peak of the derivative of the photodiode signal for the case of the coated filament is shifted from the peak visible on the derivative of the pyrometer curve. Thus, the onset of the derivative peak on the photodiode curve is interpreted as the ignition moment.

The time interval used for calculation of derivatives varied for different heating rates. A short interval (7 ms) was used for the high heating rates and long (30 ms), for the low heating rate.

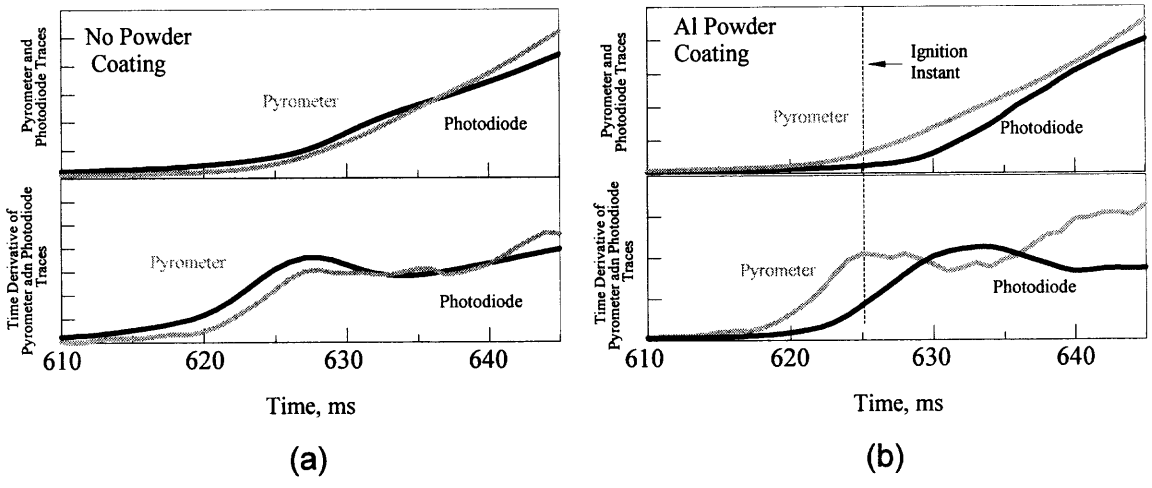

Figure 2.9 Comparison of photodiode and pyrometer channel signal.
Top: Original signals. Bottom: Derivatives. (a) Without powder on the filament (both pyrometer & photodiode focused on filament), (b) With powder coating (Pyrometer focused on filament & photodiode on powder).
Heating Rate is about 15,000 K/s.

Determination of Filament Temperature:

Two channels (channel A, 500 nm and C, 610 nm) of the pyrometer were used to determine filament temperature near the ignition instant in this project. The third channel (channel B, 568 nm) became super saturated before the ignition of aluminum. The temperature curve recorded with the third channel (up to saturation) was in good agreement with the temperature curve implied by the other two channels.

Definition and Calculation of Heating Rates:

Two approaches were used to calculate the heating rate of the filament:

1) Pre-Ignition Heating Rate

2) Average Heating Rate

The pre-Ignition heating rate is the rate of heating of the powder coating just before the ignition instant, t_i. A base interval of time, Δt was selected as the time of heating the filament by a predetermined temperature intervals ΔT prior to the ignition instant as illustrated in Figure 2.10, i.e.

$$\text{Pre-Ignition Heating Rate} = \Delta T / \Delta t$$

The ΔT was selected to be 50 K for low heating rate (around 3000 K/s) and 100 K for higher heating rates (around 9000 K/s and 16000 K/s) respectively. The average heating rate used, is the rate of the powder coating heating given by the total temperature rise from room temperature (T_i - 300K) till the moment of ignition divided by the total filament heating time, t_i, need to reach the ignition, i.e.

$$\text{Average Heating Rate} = (T_i - 300) / t_i$$

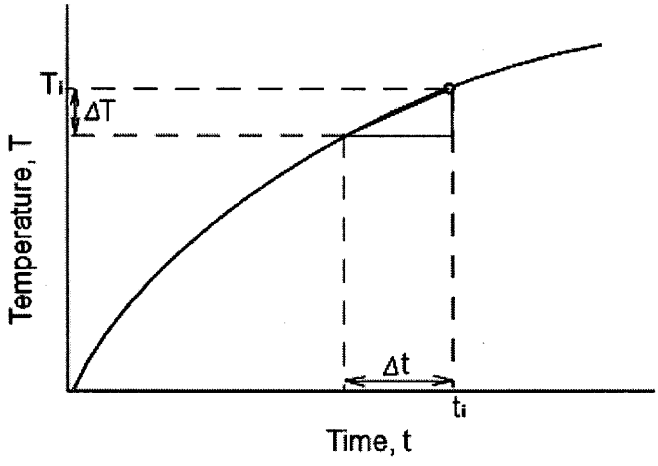

Figure 2.10 Calculation of pre-ignition heating rate.

The initial approach was to use the pre-ignition rate but it was not well reproducible, experimentally. The average heating rate was more reproducible and took into account the total history of heating the powder from the room temperature.

Table 2.1 shows the experimental parameters used in different measurement techniques and corresponding pre-ignition and average heating rates.

Table 2.1 Experimental Setup and Heating Rate Data

Heating Rate Setup				Base Temperature Interval for Heating Rate Calculations, ΔT, K	Approximate Heating Rates Obtained	
Voltage Applied Across Filament, V	Particle Size of Al Powder, μm	Carbon Filament Length mm	Technique Used		Pre-Ignition Heating Rate K/s	Average Heating Rate K/s
24	10 - 14	53 ± 1	Pyrometer	50	2,000 ± 600	2,700± 150
36	10 - 14	53 ± 1	Pyrometer	100	5,800 ± 1750	7,000 ±350
48	10 - 14	53 ± 1	Pyrometer	100	11,500±1750	12,500 ±450
48	3 – 4.5	53 ± 1	Pyrometer	100	*8,500±1100	13,300±400
36	3 – 4.5	53 ± 1	Camera	~ 50	*7,000±200	9,000±400
48	3 – 4.5	53 ± 1	Camera	~ 50	*13,700±700	16,700±600
48	3 – 4.5	30 ± 1	Camera	~ 50	*25,000±2800	40,000±1200

* Data not used in result interpretations due to inaccurate pre-ignition rate.

2.5 High-Speed Camera Technique

2.5.1 Experimental Setup & Procedures

The high speed camera used the following parameters.

Scan Rate : 500 fps

Resolution : 1280x256 pxi

Exposure time : 6 μs, 320 μs, and 332 μs

Different exposure times were used for experiments with different heating rates. (see Table 2.2)

Table 2.2 Camera Exposure Time and Heating Rates

Camera Exposure Time μs	Averaged Heating Rate K/s
6	40,000
320	17,000
332	9,000

The camera was focused on the filament with the powder coating in the center of the image. The aperture, magnification and focus of the camera were fixed for each exposure time, and camera temperature calibrations were done with the same settings. The camera was triggered externally using an analog voltage signal form a high resistance voltage divider across the filament, in the same way as was used for triggering the DAQ card for the pyrometer technique (see cable PFI0 in Figure 2.6). Filament current and voltage were not measured in these experiments.

2.5.2 Data Collection and Processing

A typical run with the camera technique includes around 200 frames while only 10-15 frames were selected for further processing. The relevant frames are those in which the image of the filament surface is not saturated. The appropriate exposure time for any particular heating rate was selected after several trials. This adjustment was needed to produce frames showing an ignition moment and showing a non-saturated image of the filament surface at the same time. The ignition frame was identified either by a visible vapor phase flame (Figure 2.11),

visible in high heating rate experiments, or a sudden increase in the brightness of the powder coating (Figure 2.12), visible in low heating rate experiments. Only one of the two modes of detection mechanism was visible in any of the performed experiments. The temperature of a filament was obtained through measuring the average intensity of the filament surface, and comparing the average intensity with calibration values (See chapter 3, Temperature Calibrations). Tracker software (Version 3) was used for the brightness intensity measurements. We measured average intensity of a square area of interest (AOI) having 100 pixels (10x10) at four different points on the filament surface (Figure 2.13). Measuring the average intensity i.e. the temperature at four different points minimized the morphology effect resulting in the variable filament image brightness due to the non-uniformity of the filament surface. For the pyrometer measurements, ratios of signals at different wavelengths were utilized to determine the temperature, which did not depend on the size of the emitting surface.

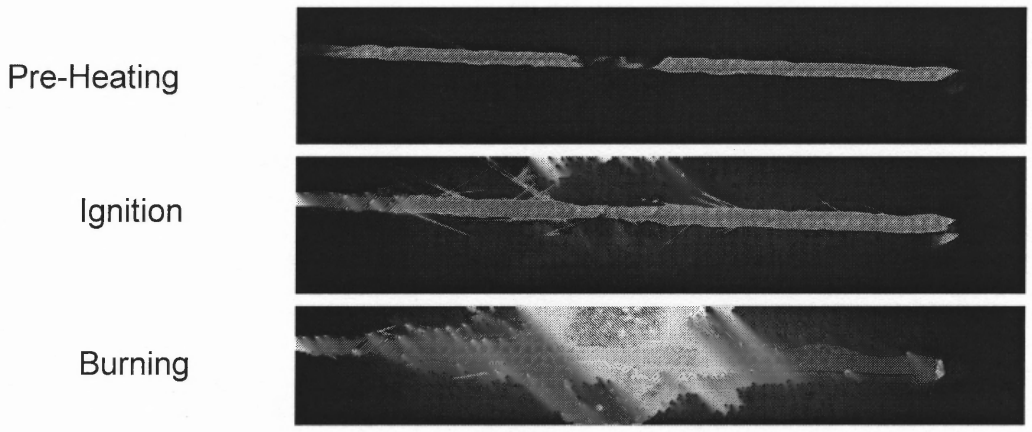

Figure 2.11 Ignition identified by the onset of vapor phase ignition. Heating rate around 40,000 K/s.

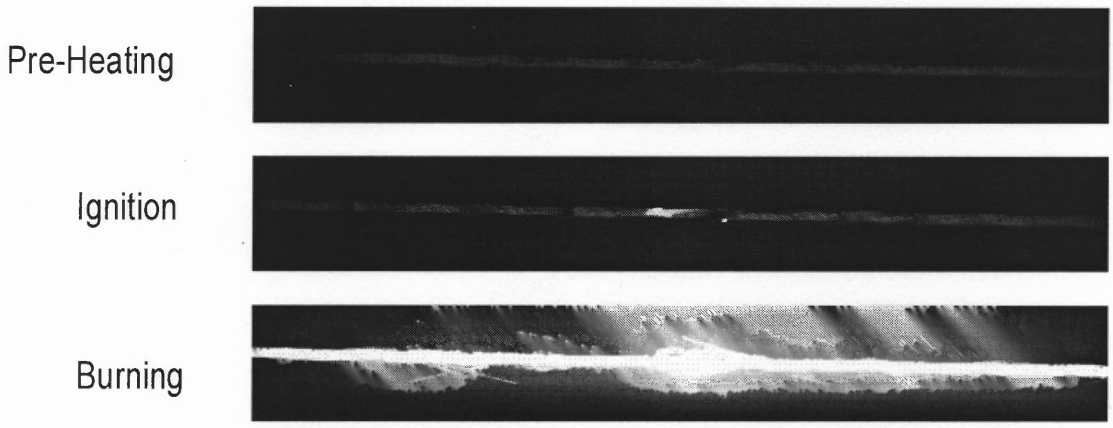

Figure 2.12 Ignition identified by the sudden rise in powder brightness. Heating rate around – 9,000 K/s

Figure 2.13 AOI location on filament image. Image shows placement of powder coating in the middle of the filament. The four small squares on the filament are the Area of Interest (AOI) selected for processing the filament image for temperature determination.

Heating Rate Calculations:

Pre-Ignition and Average heating rate (see Table 2.1) were also calculated for the camera technique. However, due to a narrow dynamic temperature range (the temperature range that can be measured without changing the settings) of the high-speed camera, the pre-ignition heating rate could not be calculated for the setting with the highest heating rate.

CHAPTER 3

TEMPERATURE CALIBRATION SETUPS AND PROCEDURES

3.1 Introduction

The experimental study used a three-color pyrometer and a high-speed camera to measure temperature. A tungsten ribbon filament strip lamp was used to calibrate the temperature measuring devices. The three-color pyrometer was calibrated for two different temperature ranges while the high-speed camera was calibrated each time for specific settings used in experiments.

3.2 Calibration Standard and Specifications

3.2.1 Tungsten Ribbon Strip Lamp Specifications

Make:	The Pyrometer Instrument Co., Inc.
Description:	Tungsten Ribbon Filament Strip Lamp
Model No.:	RSL2000
Serial No.:	975
Date of Calibration:	11/06/2002
Date of Next Calibration:	11/06/2003

Maximum allowable filament current: 30A

The manufacturer calibration data was plotted, Figure 3.1, and fitted with a polynomial trend line. The equation was used to calculate the filament temperature. The equation is given as

$$T = (-0.0000724901088986485 * A^6) + (0.00939494236825595 * A^5) - (0.499693684568718 * A^4) + (13.9812801092615 * A^3) - (218.300731814465 * A^2) + (1880.39970895716 * A) - 5815.71026076397 \quad (3.1)$$

where,

T = Temperature of the specified area on the strip lamp filament.

A = Current through tungsten strip lamp filament.

The calibration equation was adjusted for the Kelvin scale of temperature when used in the templates.

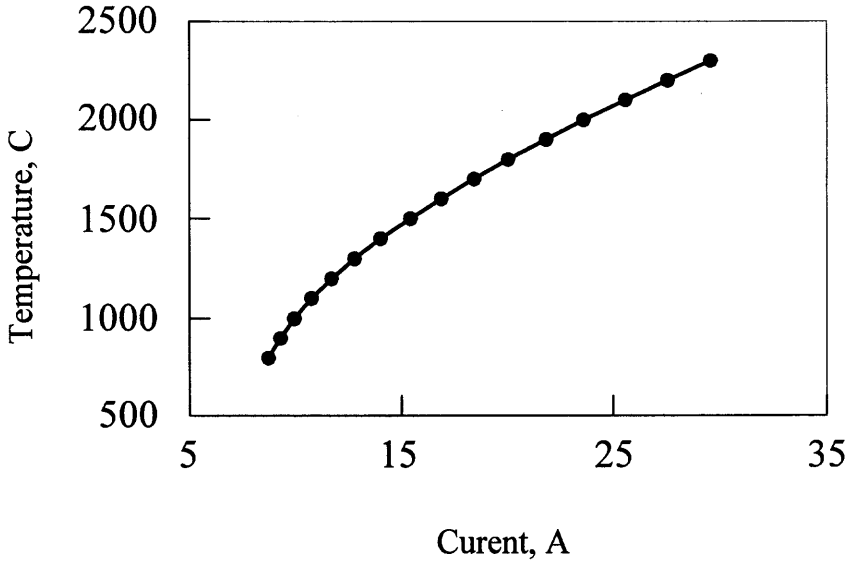

Figure 3.1 Manufacturer data for strip lamp filament; temperature and current through the filament.

3.2.2 Calibration Ranges

The pyrometer was calibrated for two ranges –

1. Low Temperature Range (1700 K – 2000 K)
2. High Temperature Range (1950 K -- 2500K)

The high-speed camera was calibrated for each specific experimental setting. The magnification and aperture were not recorded, so the calibration for each specific setting was performed immediately after the actual ignition measurement during which these settings were used. To refer to different calibrations we used exposure times (Table 3.1)

Table 3.1 Temperature Calibration Range for Camera

Camera Exposure Time μs	Temperature Calibration Range K
332	1450 - 1700
320	1500 - 1700
6	2150 - 2450

Total Range and Dynamic Range of Temperature Calibration:

The total range of a temperature measurement technique is used to indicate the possible lowest and highest temperature that could be measured with the respective technique. The dynamic range is used to imply the lowest and highest temperature that can be measured during a single experiment.

The lower limit of the total range for the pyrometer was restricted by the minimum voltage signal (15 mV) required to overcome the noise of the pyrometer electrical circuit. The upper limit was just a limit of the calibration source i.e. tungsten strip lamp. The voltage signals measurement range of the data acquisition board, 0 – 10 V, determined the dynamic range.

For the high-speed camera, the range of the calibration source, the tungsten strip lamp, limited the total range. The dynamic range was restricted due to the pixel brightness saturation at a particular time and aperture setting. The respective ranges are given in Table 3.2.

Table 3.2 Calibration Ranges for Pyrometer and Camera

	Total Range K	**Dynamic Range K**
Three Color Pyrometer	1700 – 200	500
High Speed Camera	1100 - 2600	250

3.3 Temperature Calibration of the Three Color Pyrometer

Energy radiated by any black body for a particular wavelength, $E_{b\lambda}$, is given as [14]: -

$$E_{b\lambda} = \frac{C_1 \lambda^{-5}}{e^{C_2 / \lambda T} - 1} \tag{3.2}$$

where, λ is the wavelength, T is the temperature and C_1, C_2 are constants, equal to 3.743×10^8 Wμ/m^2 and 1.4387×10^4 μmK , respectively.

Ratio of the energies associated with any two wavelengths can be expressed as;

$$\frac{E_{b\lambda_1}}{E_{b\lambda_2}} = \left[\frac{\lambda_2}{\lambda_1}\right]^5 \left[\frac{e^{C_2/\lambda_2 T} - 1}{e^{C_2/\lambda_1 T} - 1}\right] \tag{3.3}$$

The ratio of the energies given above (Eq. 3.3) is for a black body. It can also be used to describe the ratio of energies for a gray body. We assumed the graphite filament used in the project, to be a gray body. To measure the temperature of any surface, we need to know surface radiation energy associated with two different wavelengths. The three-color pyrometer measures the energy emitted at three wavelengths. Any two of the three signals recorded can be used to measure the temperature. It is advantageous to use three channels instead of two.

Advantages of using all three wavelengths:

1. Radiation energies associated with different wavelengths vary in a very wide range. Many times, the signal value (voltage signal associated with the energy) goes out of the range of the measuring equipment. Use of three wavelengths widens the working range of the pyrometer as different pairs of channels (i.e. wavelengths) can be selected for different ranges of temperature.
2. A set of three channels gives three possible combinations of ratios i.e. three different ways of measuring the same temperature. Use of the three ratios is helpful in determining if any of the three channels is deviating from the gray body

behavior. The wavelengths selected for the channel used in the pyrometer (500 nm,568 nm, & 610 nm) did not coincides with the characteristic emission wavelengths of carbon or aluminum, [15].

3.3.1 Experimental Setup

The experimental setup included a tungsten ribbon filament strip lamp, variable resistance box, 12 V DC power source, a three-color pyrometer and a National Instrument data collection system.

Focusing and Alignments:

Figure 3.2 shows the experimental setup used for pyrometer calibration. An adjustable slit was used to restrict the pyrometer's field of view, only to the specified area of the tungsten strip filament. The strip lamp is calibrated by the manufacturer to produce a predetermined temperature only at a given area on the tungsten strip filament (indicated by a wire mark next to the area). A laser beam was used to align the pyrometer, strip lamp filament, and adjustable slit. The strip filament was aligned perpendicularly to the axis of the setup.

The distance between the strip lamp ribbon and adjustable slit, a, and adjustable slit and three color pyrometer, b, (see Figure 3.2) for two different calibrations performed were as follows –

(1) Low Temperature (1700 K – 2000 K) a = 7.3 cm b = 20.3 cm

(2) High Temperature (1950 K – 2500 K) a =7.3 cm b = 36.8 cm

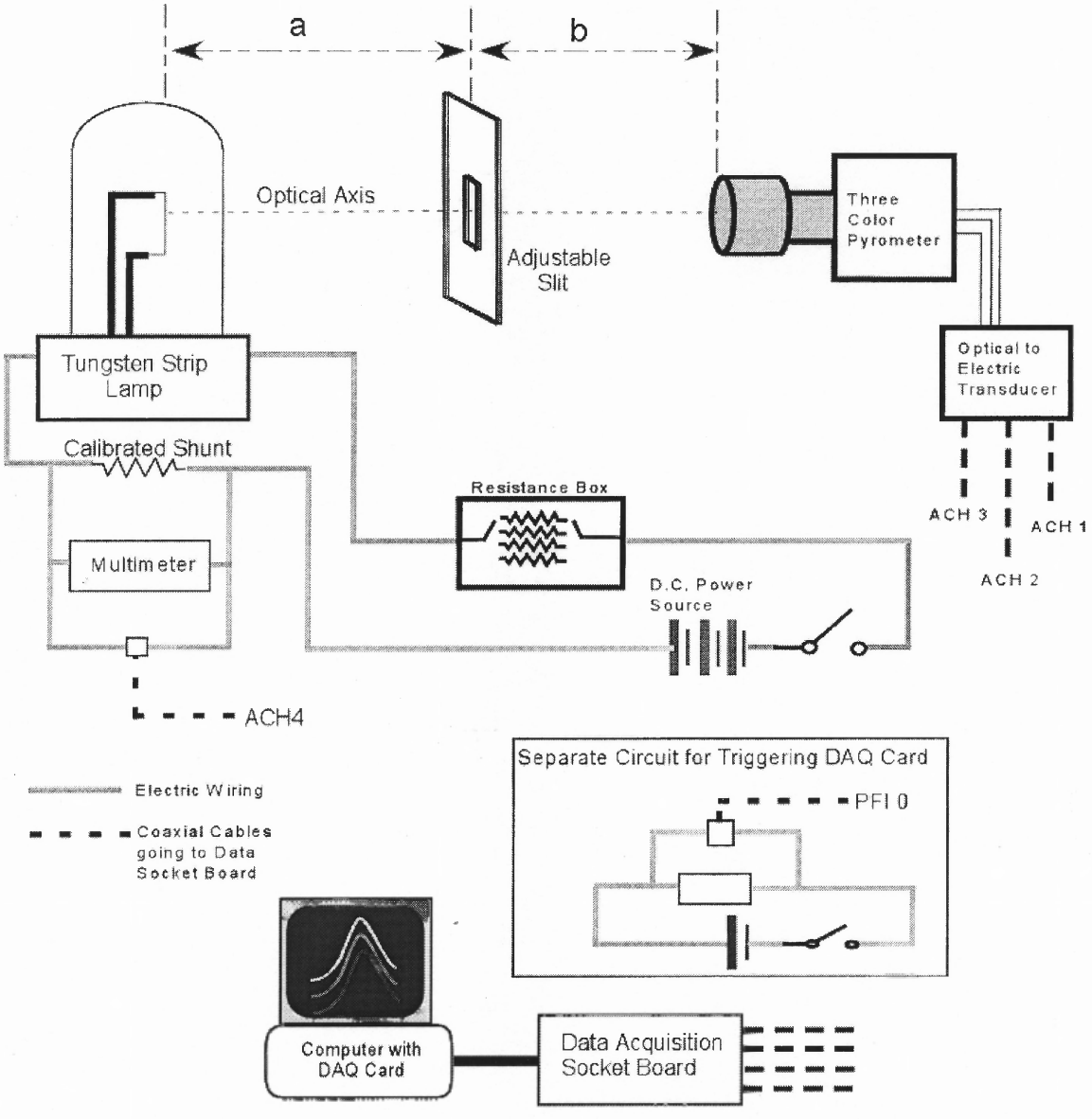

Figure 3.2 Schematic diagram of experimental setup and electrical connections for temperature calibration of three-channel pyrometer.

Electrical Connections

The DAQ card measured three signals: (Figure 3.2), from three channels of the pyrometer, using terminals ACH1, ACH2 and ACH3 of the data socket board (see Figure 2.5). The data acquisition socket board was connected to the

DAQ card installed in the computer. A separate scheme was used to trigger the DAQ card. The current through the strip lamp filament was measured by a multimeter (TECHMASTER$_{TM}$ DM-8400) (maximum sensitivity of 0.1mV), by measuring the voltage across a calibrated resistance (I mΩ). This voltage was also recorded by the DAQ card, using terminal ACH 4.

3.3.2 Data Collection and Processing

The data were recorded at 1000 sps and then stored in an excel file, as four columns representing the data from signals from three pyrometer channels and a voltage across the calibrated resistor. The filament current was measured manually with a multimeter. All the signals measured here were in a steady state so the data were recorded for a 100 ms time interval and the average values were used to represent steady state value. The average value of the radiation intensity for each pyrometer channel (A for 500 nm, B for 568 nm and C for 610 nm) was obtained for each value of the filament temperature (T) (calculated from the current in the filament, see section. 3.2.1). The filament current measured manually with the multimeter was used for the temperature calculations. These measurements were repeated with different filament currents (i.e. temperatures), using a variable resistance box (maximum resistance, 1 Ω) to vary the filament current. Three ratios, B/A, B/C and A/C, of the average channel values for each run were calculated. These three ratios were plotted against the inverse of the corresponding filament temperature (1/T).

Each data set was fitted with a logarithmic trend line (following the theoretical trend predicted by the equation 3.2). Figure 3.3 shows a typical plot of all three ratios for every run, for a low temperature range. Figure 3.4 represents a similar plot for the high temperature range. The fitting produced three logarithmic equations, one corresponding to each ratio. These equations (Table 3.3) can be used to calculate the temperature, from the recorded signals of each couple of the pyrometer channels.

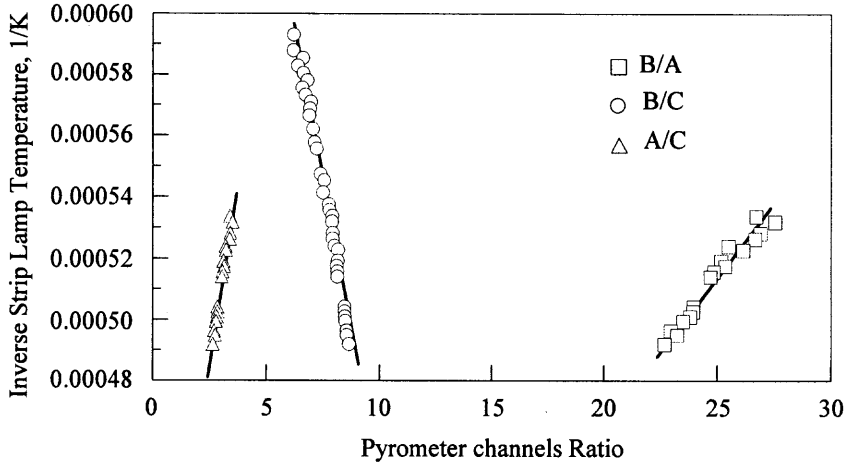

Figure 3.3 *Pyrometer calibration plot for low temperature range (1700-2000K). Distance between the pyrometer and strip lamp was 27.6 cm.*

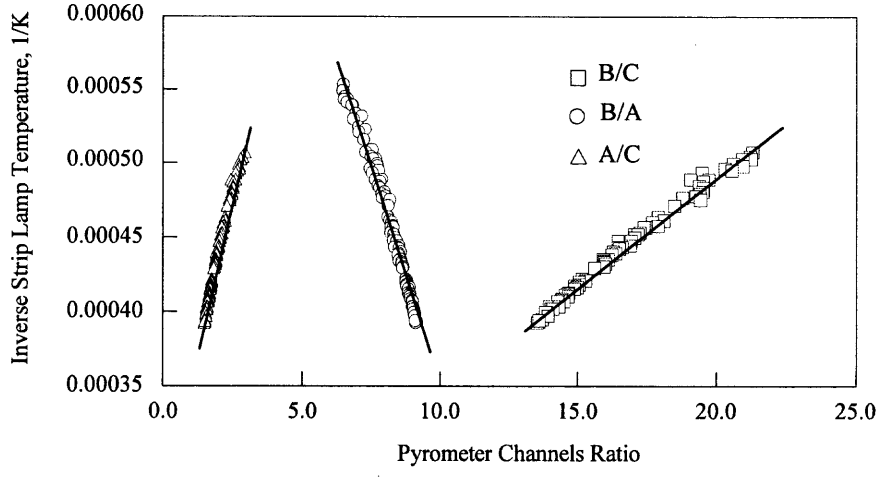

Figure 3.4 Pyrometer calibration plot for high temperature range (1700 K-2000K). Distance between the pyrometer and strip lamp was 44.1 cm.

3.3.3 Result - Calibration Equations

The pyrometer was calibrated for two different temperature ranges (Figure 3.3 & 3.4) that resulted in six calibration equations, three for each range. Table 3.3 lists all the six equations. In the project only one of the six equations was used because only two channels, A and C, never saturated during the temperature measurements.

Table 3.3 Calibration Equations for Three Color Pyrometer

Calibration Range 1700 – 2000 K	
*** Channels Ratio**	**Calibration equation**
B/A	T = 1/(-0.000298704619911654*LnB/A+0.0011433052857503)
B/C	T = 1/(0.000223731434859556*Ln B/C-.00020577951375202)
**** A/C**	T = 1/(0.00014919096676301*LnA/C+0.00034810407543221)
Calibration Range 1950 – 2500 K	
Channels Ratio	**Calibration equation**
B/A	T = 1/(-0.00047218171328681 7*Ln B/A+0.001446926687955)
B/C	T = 1/(0.000250184339991888*Ln B/C-0.0002588651037540)
A/C	T = 1/(0.00017386488003868*Ln A/C+0.0003252817293015)

* A – 500nm, B – 568 nm, C – 610 nm.

** This equation was used in this project.

3.4 Temperature Calibration of High Speed Camera

The graphite filament and the tungsten ribbon strip lamp filament used in this project are assumed to be gray bodies, with the emissivity constant, not depending on the temperature. For the temperature ranges of interest (1400 – 2000), the emissivities of tungsten and graphite are equal to 0.90 [13] and 0.45 [15] respectively. The camera was calibrated for each setting used in experiments. A total of three settings were used in this project (due to different camera exposure time). The radiation intensity from the hot carbon filament surface was compared with the radiation intensity from the hot strip lamp filament surface, that is a surface with the known temperature. Before the comparison, the radiation intensities were adjusted with respect to the emissivities of the surface of graphite and tungsten, respectively

3.4.1 Experimental Setup

As shown in Figure 3.6, the temperature calibration setup for the high-speed camera included the camera with respective computer board software, the tungsten ribbon strip lamp, variable resistance box, a 12 V D.C. power source and a multimeter. The resistance box is used to vary the current through (and the temperature of) the strip filament. The calibration for a particular camera setting starts with the positioning the camera with the same settings (focus, magnification, and aperture), which were used in the actual ignition experiment. The camera and the strip lamp are fixed in a position that gives sharp image of the strip filament. The camera was triggered manually using the camera

software. The current through the strip lamp was measured with a multimeter in the same manner as was done for the pyrometer calibrations.

3.4.2 Data Collection and Processing

The data collection for the temperature calibration of the high-speed camera begins with determining of the lowest temperature that the camera is able to record with the given settings. Once that is done, the camera is made to records fifty frames at a given filament temperature, at 500 sps. Only each sixth frame was recorded and later processed. The idea behind skipping five frames after every recorded frame was to collect a shorter sample from a set of around 50 frames to reduce the use of the computer memory in the data processing. These eight-recorded frames were processed using Tracker (Version 3) software. The processing of these eight frames involved first locating the region on the surface of strip lamp filament that was calibrated by the manufacturer for temperature (indicated by a wire mark near the strip filament) and then drawing a square Area of Interest (AOI) having 100 pixels (10 x 10), using the software tool, see Figure 3.5. The software allows one to measure the minimum, maximum and average intensity of brightness of the pixels in the area of interest. The average value of the intensity was taken as we used 100 pixels, which was assumed enough to take into account of any pixel-to-pixel variation in the AOI. This measurement was performed for all eight frames and stored in an excel file. This process was repeated for different temperatures of the strip lamp filament (by varying the current). The measurements were done until the saturation of the image of the hot strip filament.

The collected data, gave the strip lamp filament intensity for different temperatures. But as this calibration is to be used for the temperature measurement of the carbon filament surface, with a different emissivity, 0.9 [13] than the emissivity of strip lamp filament surface, 0.45 [15]. Thus, intensity measured above was multiplied by a factor, 0.9/0.45 = 2, to make it compatible with carbon the filament surface. The resulted data were plotted and fitted with a power curve, see Figure 3.7. The equation of this trend line was used to calculate the temperature of the carbon filament. (See section 3.4.3)

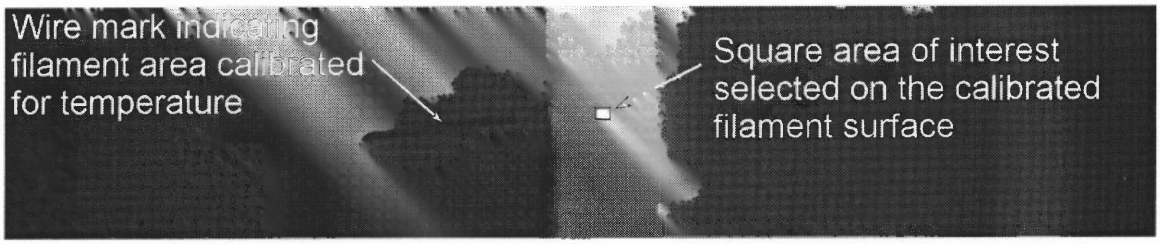

Figure 3.5 Selection of Area of Interest (AOI) on the strip lamp filament surface.

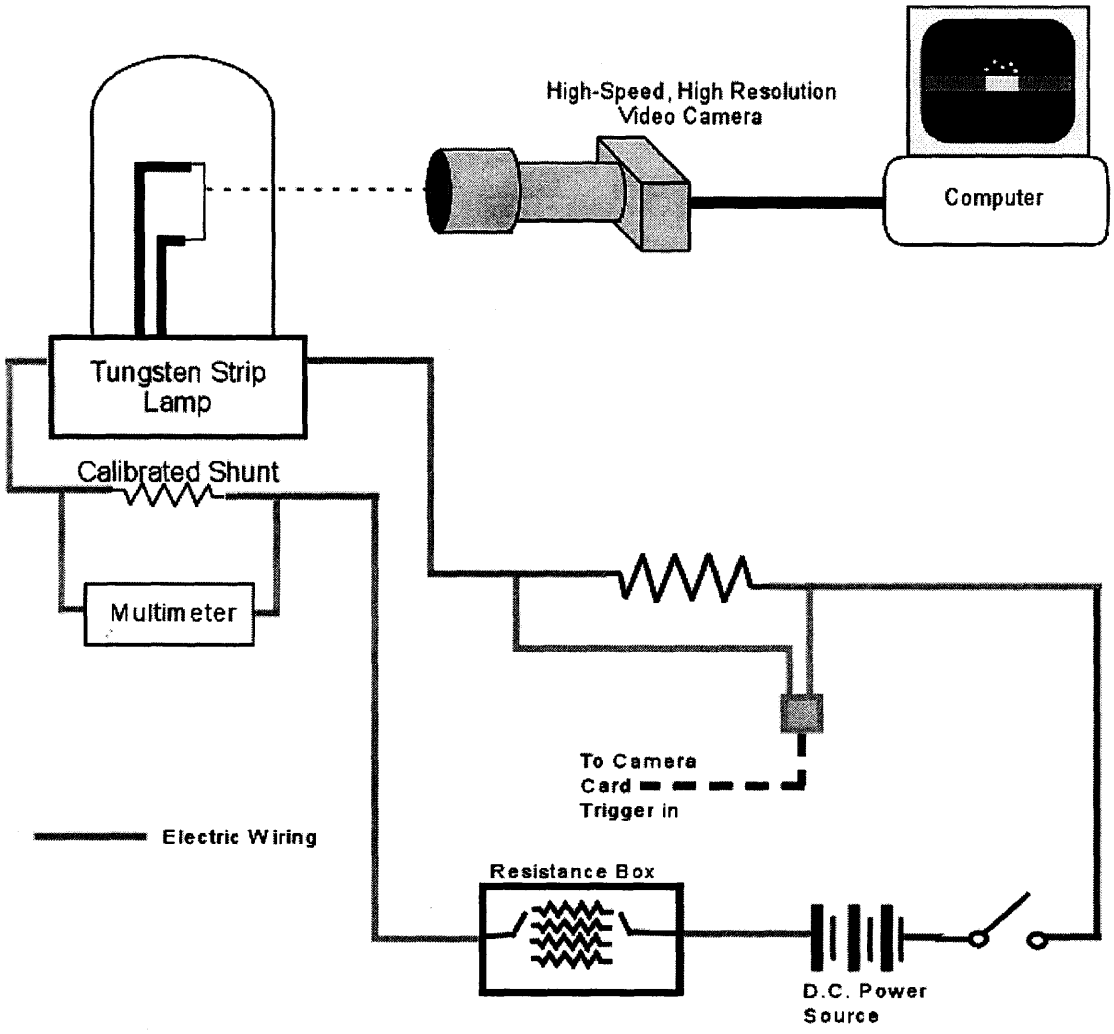

Figure 3.6 Experimental Setup for the temperature calibrations of the high-speed camera.

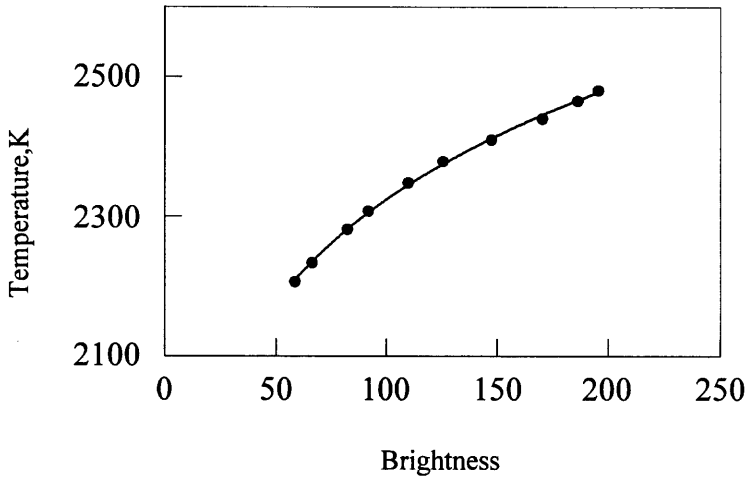

Figure 3.7 Temp Vs Brightness – Calibration plot of high-speed camera for 6 μs exposure timing.

3.4.3 Results – Calibration Equations

Calibration was repeated for three different camera setting. Table 3.4 gives the calibration equations derived for different settings.

Table 3.4 Calibration Equations for High-Speed Camera

Camera Exposure Time μs)	Temperature Calibration Range (K)	Calibration Equation	Heating Rates Used in Exp. K/s
332	1450 - 1700	$T = 952.469717055832 * I^{0.10558856481384100}$	9,000
320	1500 - 1700	$T = 1133.44205263743 * I^{0.06683191048904320}$	17,000
6	2150 - 2450	$T = 365.02543146014 * I^{0.114385653493857}$	40,000

3.5 Error Estimation In Temperature Calibration

The error common to both the pyrometer and camera calibration originated from the limitation in the measurement the strip lamp current. The multimeter used has a sensitivity of 0.1 mV that corresponds to 0.1 A error in the estimation of strip lamp filament current. A calibrated shunt of I mΩ was used to measure the current (See Figure 3.2 and 3.6). An error of 0.1 A gave an error of 8 k, using the manufacturer calibration data for strip lamp (Eq. 3.1). In addition to the error during the calibration, other experimental error resulted from focusing of the device i.e. the area of view. The random experimental errors and the systematic errors were eliminated in the analysis by repeating many experiments and using the standard deviation as the total error bars for the measurements.

CHAPTER 4

RESULTS AND DISCUSSION

Results of ignition temperature dependence on heating rate for two different particle size aluminum powders, 10 – 14 μm and 3 – 4.5 μm, are presented here. The investigation of the two powders showed a dependence of the aluminum ignition temperature on particle size. For both particle sizes, a higher ignition temperature for higher heating rate was observed. For the same heating rate, the powders with larger particles ignited at higher temperatures.

4.1 Results and Discussion Al (10-14)

Table 4.1 shows the summary for the results of Al powder with the averagel particle size of 10-14 μm. Results for three different heating rates corresponding to three different experimental settings are presented. Both the pre-ignition and averaged heating rates are shown. All the temperature measurements for the 10-14 μm powder were conducted with the pyrometer technique.

Figure 4.1 shows a comparison of the pre-ignition and averaged heating rates. The spread of points (along x-axis) with pre-ignition heating rate is more than that with average heating rate. This is attributed to better experimental reproducibility of the average heating rate. Results for both heating rates follow the trend of higher ignition temperatures for higher heating rates.

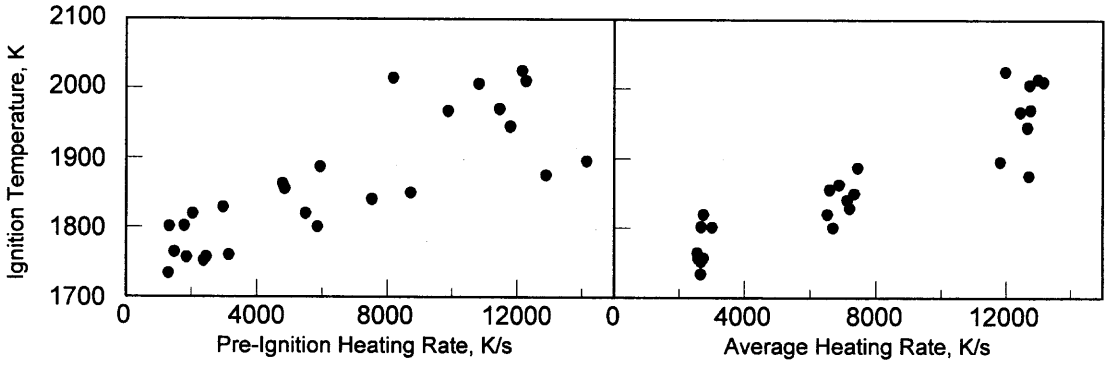

Figure 4.1 Ignition Temperature Dependence on heating Rates for Al 10-14 μm.

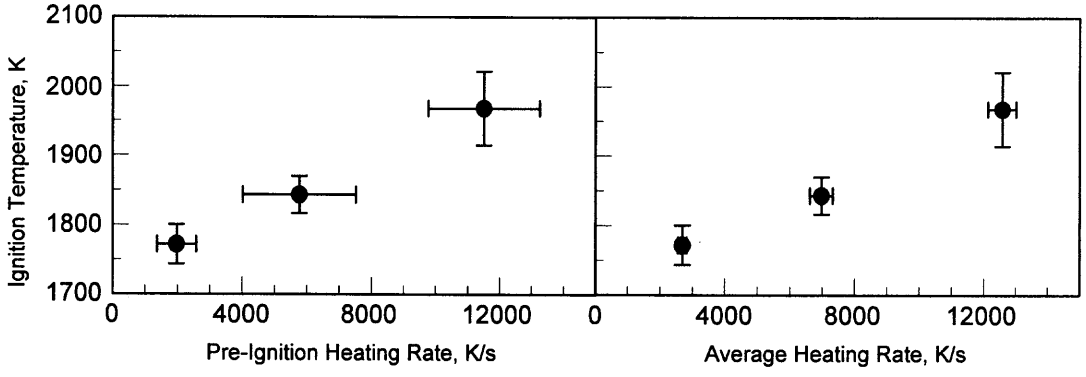

Figure 4.2 Comparison of average and pre-ignition heating rates for Al 10-14 μm. The average heating rate shows smaller error bars indicating the better experimental reproducibility.

Figure 4.2 represents the data shown in Figure 4.1 where each experimental setting is represented by a single point. The standard deviation is used as the error bar for this representative points. The error bar for both, pre-ignition and average heating rates do not overlap. The error bars for pre-ignition heating rate are larger than those for average heating rates.

Table 4.1 Experimental Results for Al 10-14μm Powder (Measured with Pyrometer Technique)

Pre-Ignition Heating Rate. K/s	Average Heating Rate K/s	Ignition Temperature K
2045	2747	1819
1490	2560	1764
1790	2676	1802
2460	2579	1757
1307	2661	1734
1862	2738	1757
2380	2669	1752
3147	2594	1760
1340	3008	1801
8715	7344	1850
5933	7451	1887
7521	7131	1840
2977	7211	1829
5859	6700	1801
4847	6591	1855
4785	6885	1863
5490	6524	1820
11792	12657	1945
12898	12705	1875
10822	12733	2006
9869	12445	1968
14148	11822	1896
12159	11982	2025
12277	13159	2011
8181	12989	2015
11464	12752	1971

4.2 Results and Discussion Al 3 – 4.5 μm

Table 4.2 gives the summary of results for aluminum powder of 3 – 4.5 μm average particle size. Three different heating rate ranges, corresponding to three different experimental settings are presented. All temperature measurements

were conducted using the camera technique with the pyrometer used additionally for one experimental setting.

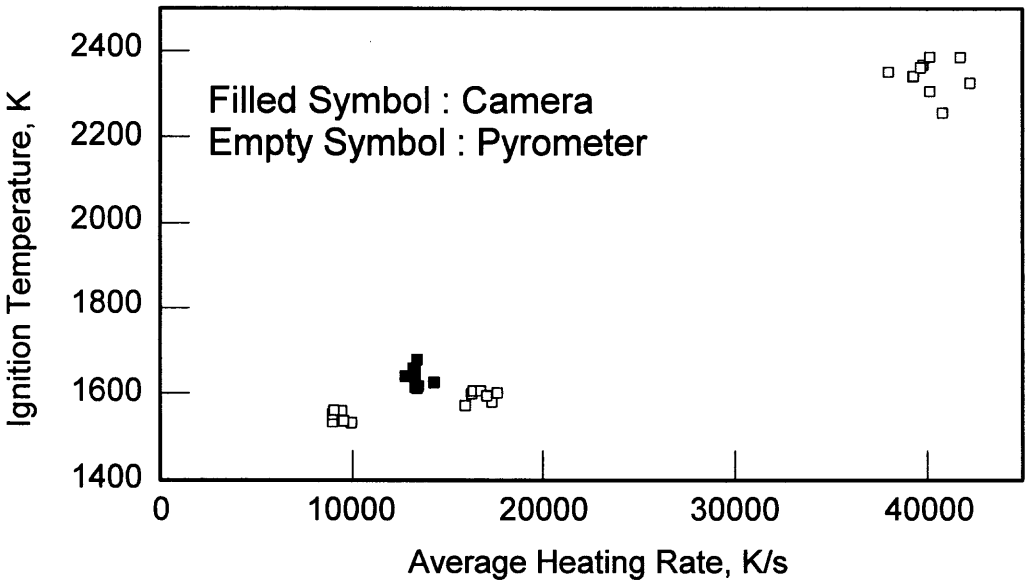

Figure 4.3 Ignition rate dependence on heating rates for Al 3 – 4.5 μm.

Figure 4.3 shows the results of ignition temperature dependence on heating rates for Al 3 – 4.5 μm. Results were interpreted only on the basis of the average heating rate because it was not possible to calculate the pre-ignition heating rate for camera technique used. This was because of the narrow dynamic temperature range for high-speed camera resulting in a very small temperature range that could be measured from the same image sequence. The experiments for the intermediate heating rates were also performed with the pyrometer technique. Although the pyrometer was not calibrated for such low temperature, the same pyrometer temperature calibration equation (see Table 3.3) was used to extrapolate the calibration curve. Due to limited measured

temperature range, only the average heating rate could be calculated accurately. Thus average heating rate was used for comparative analysis to maintain consistency.

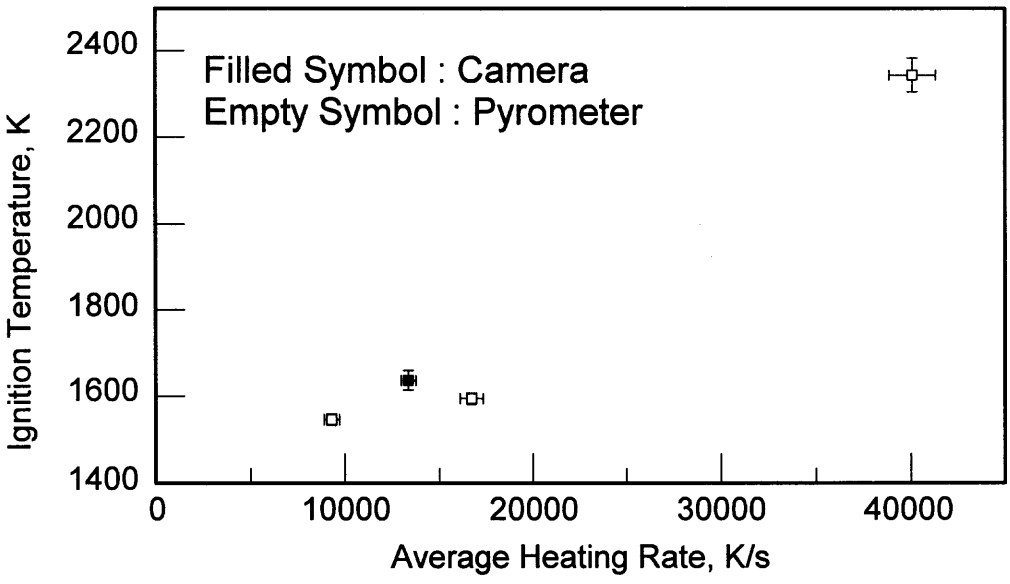

Figure 4.4 Ignition Temperature as a function of the average heating rate for Al 3 – 4.5 μm.

For the finer particles the points from the two techniques (with the same experimental settings) are shifted horizontally (see Figure 4.3), which could be interpreted assuming that the pyrometer and camera registered events that were slightly shifted in time. But both clusters of experimental data points lie close to each other implying that both events are closely timed. Figure 4.4 shows the results presented in Figure 4.3 where an average ignition temperature is shown for each experimental setting. The error bars represent standard deviations for each point. Both Figures 4.3 and 4.4 show a consistent trend of an increase in ignition temperature with the rise in the heating rate.

Table 4.2 *Experimental Results for Al 3 – 4.5 μm using Camera and Pyrometer Technique*

Pre-Ignition Heating Rate. K/s	Average Heating Rate K/s	Ignition Temperature K	
7216	8950	1535	Camera Technique
6988	9939	1532	
7183	9402	1560	
6790	9515	1537	
7298	8942	1552	
6848	9007	1561	
7216	8950	1535	
12325	15905	1572	
14095	16242	1599	
14317	16325	1606	
13607	17311	1581	
13693	16738	1606	
14440	17589	1602	
13650	17041	1595	
26388	40766	2257	
28965	42210	2326	
25189	37983	2351	
23241	39241	2341	
27324	39263	2342	
23184	40131	2307	
25470	41716	2386	
18721	39768	2368	
24618	39639	2361	
26229	40125	2387	
8821	13264	1653	Pyrometer Technique
8141	13182	1658	
9465	13284	1615	
6656	13391	1612	
10332	13432	1616	
7579	13380	1678	
9025	14253	1626	
8317	13284	1628	
9546	12757	1639	

4.3 Effect of Aluminum Particle Size on Ignition Temperature

Figure 4.5 shows ignition temperatures for two particle sizes fractions of Al plotted versus average heating rate. The comparisons in Figure 4.5 indicate ignition of the smaller particles of aluminum at a lower temperatures than larger particles at the same heating rate. Both the powder fractions show higher ignition temperatures for higher heating rates.

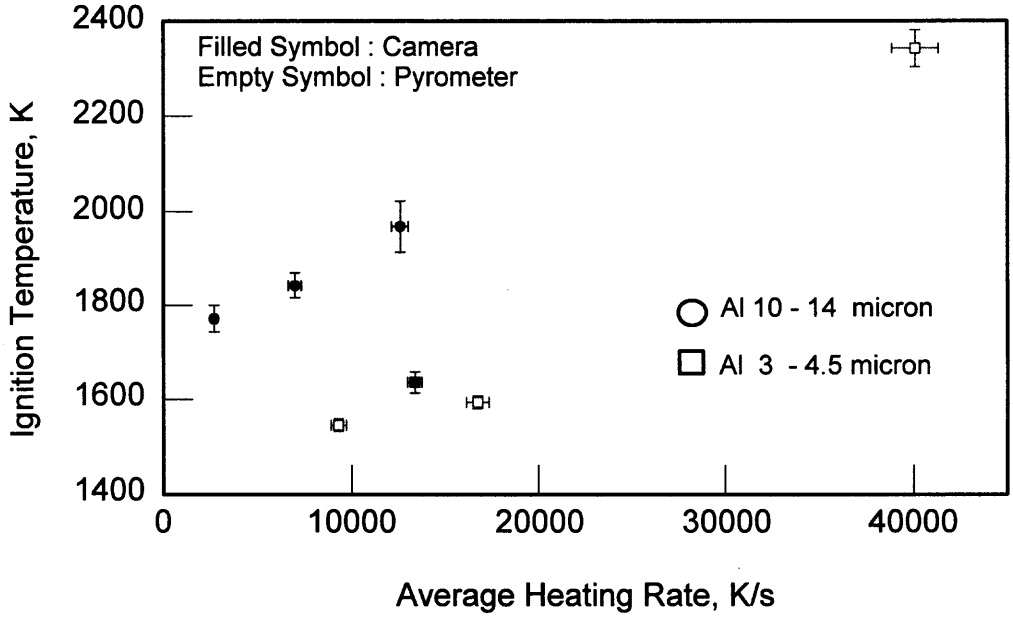

Figure 4.5 Ignition temperature dependence on heating rate and particle size.

4.4 Comparison of Measured Ignition Temperature with the Literature Data

Figure 4.6 plots the obtained ignition temperatures for two particle sizes of aluminum powder with the results published by other authors. The present results show different ignition temperatures for the same particle size, which can be explained on the basis of different heating rates employed. A discrepancy is visible in the earlier results also and a strong effect of heating rate is clear.

However, no information was found in the literature regarding the heating rates used and thus the comparison of different results to one another is difficult.

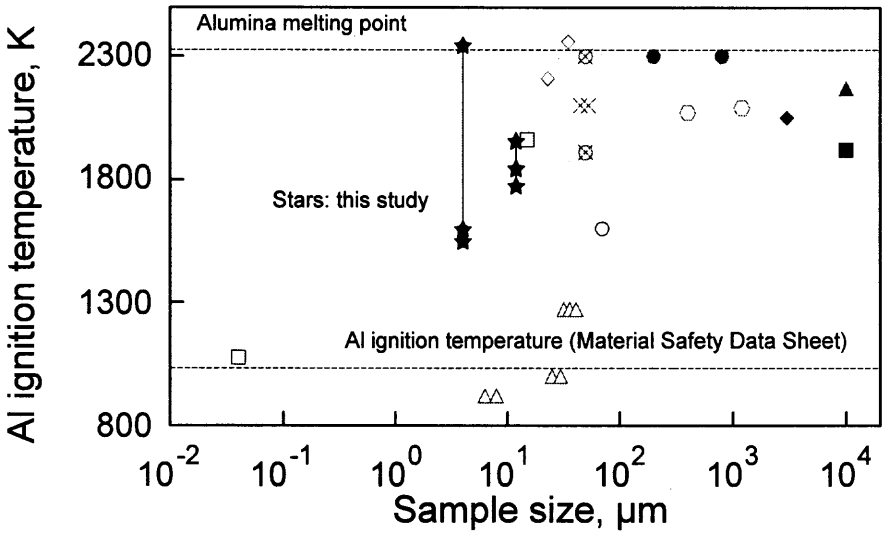

Figure 4.6 Comparison of results obtained in this work with results published by other researchers. (See Figure 1.1 for references)

The data of the present study show a trend of a lower ignition temperature for smaller particle size for the same heating rates. The results from different authors showing different ignition temperatures for the same particle size could be due to different heating rates used by different researchers.

4.5 Data Interpretation

4.5.1 Calculation of Activation Energy

The obtained data can be used to calculate aluminum ignition activation energy using Kissinger isoconversion method. The iso-conversion method relates ignition temperature with the heating rate by the following equation: -

$$\ln\frac{\alpha}{T_i^2} = -\frac{E_a}{R \cdot T_i} + C \tag{4.1}$$

where, E_a is the activation energy; Z is the pre-exponent, R is universal gas constant, α is the heating rate, C is a constant and T_i is the ignition temperature. To calculate the activation energy, experimental data obtained here are plotted in appropriate coordinate system i.e. $\ln\frac{\alpha}{T_i^2}$ versus $\frac{1}{T}$. A straight line is produced and, in accordance with Eq.(4.1), the slope of the resulting line is directly proportional to the activation energy (see Figure 4.7). One estimate using the present data for Al 10 – 14 μm, gave activation energy equal to 204 KJ/mol. This is not in the range reported by different authors earlier, i.e. from 71 to 95 kJ/mol [Yu et al. 1973, Gurevich et al. 1970, Reynolds 1959], but still is in the same general neighborhood. This discrepancy could be because the Kissinger isoconversion method estimates the activation energy taking into account the particle temperature while in this experiment the filament temperature is measured as the ignition temperature. Thus, a detailed heat transfer model is

needed to accurately interpret the present experiment, which can take into account the filament temperature.

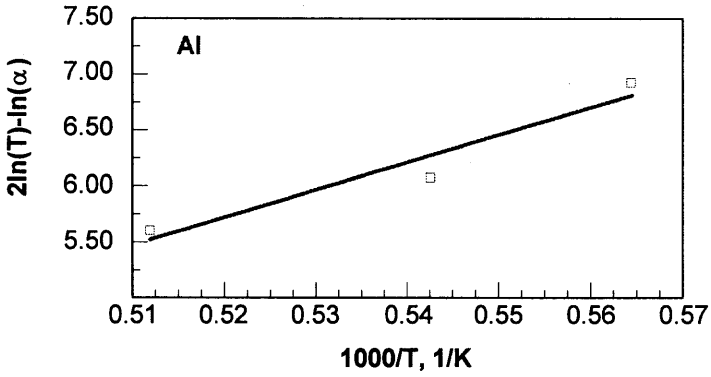

Figure 4.7 Calculation of activation energy from Kissinger Isoconversion method. The slope of the curve is proportional to activation energy.

4.5.2 Formulation of Ignition Model

A simple approach for a heat transfer model interpreting the present experiment can start with a simple assumption [16] in which the particle temperature is the balance of chemical and physical heat transfer rates.

$$c_p \cdot \rho_p \cdot V_p \frac{dT_p}{dt} = \dot{Q}_{ph}\left(t, T_p, T_e\right) + \dot{Q}_{ch}\left(t, T_p, T_e\right) \tag{4.2}$$

where the subscripts refer to as, *p* – particle, *e* – environment, *ph* –physical and *ch* – chemical

The physical heat transfer term includes all the heat transfer processes occurring with an inert particle, like convection, radiation, etc. The chemical heat transfer term accounts for heat transfer describing ignition. Any temperature

change in the physical environment affects the physical heat transfer term. Thus a systematic change in the physical environment, such as heating rate, can be employed to identify the chemical heat transfer heat transfer term from Eq. (4.2) and characterize the ignition process. A simple way to model the chemical heat transfer can be to assume it to be an Arrhenius-type expression.

$$\dot{Q}_{ch} = A \cdot \Delta H \cdot Z \cdot exp\left(-\frac{E_a}{RT_p} \right) \tag{4.3}$$

where A is the particle area and ΔH is the oxidation enthalpy. Matching the computed and experimental ignition temperatures at different heating rates can be used to estimate constants of the Arrhenius term. The ignition model developed with this approach could work for different experimental conditions.

CHAPTER 5

CONCLUSION AND FUTURE WORK

5.1 Conclusions

1) An approach for characterization of Al ignition at different heating rates has been developed.

2) Ignition of Al occurs at increasingly higher temperatures as the heating rate increases.

3) For heating rates varied from 2000 to 16000 K/s, the ignition temperatures of 10-14 μm Al powder changed from 1750 to 2000 K.

4) For heating rates varied from 16000 to 40000 K/s, the ignition temperatures of 3 - 5 μm Al powder changed from 1600 to 2300 K.

5) At the same heating rate, smaller particles ignite at lower temperature.

6) A detailed heat transfer model is necessary to better interpret present experiments and characterize Al ignition kinetics.

5.2 Future Work

In the present study, for Al 3 – 4.5 μm, the ignition temperature for highest heating rate (around 40000 K/s) is slightly above the melting point of alumina. More experiments can be conducted to find out the behavior of larger Al particles for still higher heating rates. Moreover, the dependence of the ignition temperature on the heating rate can be investigated in detail when it approaches

melting point of alumina. In addition to heating rate effect, the ignition temperature dependence on different surrounding gas environment can also be studied, which could give an additional inputs in the understanding of Al ignition kinetics and developing accurate model for Al ignition.

APPENDIX A

EXCEL FILE NAMES OF EXPERIMENTAL TEST RUNS

The names of the excel files used for data processing of the experimental runs conducted for ignition temperature determination of Aluminum powders are given here. Table A.1 and A.2 contains the excel file name list for Al10-14 μm and Al 3-4.5μm Al powders, respectively. The lists tabulate the file name according to the ignition temperatures obtained from that runs.

Table A.1 Name of Excel Files used for Al 10 – 14 μm Experimental Runs

Ignition Temperature	
k	File Name
1819	W10-14-Al-0-5-3--01.xls
1764	W10-14-Al-0-5-3--02.xls
1802	W10-14-Al-0-5-3--03.xls
1757	W10-14-Al-0-5-3--04.xls
1734	W10-14-Al-0-5-3--05.xls
1757	W10-14-Al-0-5-3--06b.xls
1752	W10-14-Al-0-5-3--07a.xls
1760	W10-14-Al-0-5-3--08a.xls
1801	W10-14-Al-0-5-3--08b.xls
1850	W10-14-Al-0(36)-5-3--01a.xls
1887	W10-14-Al-0(36)-5-3--02a.xls
1840	W10-14-Al-0(36)-5-3--02b.xls
1829	W10-14-Al-0(36)-5-3--02c.xls
1801	W10-14-Al-0(36)-5-3--02d.xls
1855	W10-14-Al-0(36)-5-3--03a.xls
1863	W10-14-Al-0(36)-5-3--03b.xls
1820	W10-14-Al-0(36)-5-3--04a.xls
1945	W10-14-Al-0(48)-5-3--01a.xls
1875	W10-14-Al-0(48)-5-3--01b.xls
2006	W10-14-Al-0(48)-5-3--01c.xls
1968	W10-14-Al-0(48)-5-3--01d.xls
1824	W10-14-Al-0(48)-5-3--01e.xls
1896	W10-14-Al-0(48)-5-3--02a.xls
2025	W10-14-Al-0(48)-5-3--03a.xls
2011	W10-14-Al-0(48)-5-3--04.xls
2015	W10-14-Al-0(48)-5-3--05.xls
1971	W10-14-Al-0(48)-5-3--06.xls

Table A.2 Name of Excel Files used for Al 3 – 4.5 μm Experimental Runs

Ignition Temperature	
k	File Name
Camera Technique	
1535	CP-3--4-5Al-(36)--03B.xls.xls
1532	CP-3--4-5Al-(36)--03D.xls.xls
1560	CP-3--4-5Al-(36)--03E.xls.xls
1537	CP-3--4-5Al-(36)--03F.xls.xls
1552	CP-3--4-5Al-(36)--03G.xls.xls
1561	CP-3--4-5Al-(36)--03H.xls.xls
1572	CP-3--4-5Al-(48)--01.xls.xls
1599	CP-3--4-5Al-(48)--03.xls.xls
1606	CP-3--4-5Al-(48)--04.xls.xls
1581	CP-3--4-5Al-(48)--07.xls.xls
1606	CP-3--4-5Al-(48)--08.xls.xls
1602	CP-3--4-5Al-(48)--010.xls.xls
1595	CP-3--4-5Al-(48)--011.xls.xls
2257	CP-3--4-5Al-(48shwr)--01.xls.xls
2326	CP-3--4-5Al-(48shwr)--02.xls.xls
2351	CP-3--4-5Al-(48shwr)--03.xls.xls
2341	CP-3--4-5Al-(48shwr)--04.xls.xls
2342	CP-3--4-5Al-(48shwr)--05.xls.xls
2307	CP-3--4-5Al-(48shwr)--06.xls.xls
2386	CP-3--4-5Al-(48shwr)--07.xls.xls
2368	CP-3--4-5Al-(48shwr)--08.xls.xls
2361	CP-3--4-5Al-(48shwr)--09.xls.xls
2387	CP-3--4-5Al-(48shwr)--10.xls.xls
Pyrometer Technique	
1653	UW3--4-5-Al-0(48)-5-3--03.xls
1658	UW3--4-5-Al-0(48)-5-3--04.xls
1615	UW3--4-5-Al-0(48)-5-3--05.xls
1612	UW3--4-5-Al-0(48)-5-3--06.xls
1616	UW3--4-5-Al-0(48)-5-3--07.xls
1678	UW3--4-5-Al-0(48)-5-3--08.xls
1626	UW3--4-5-Al-0(48)-5-3--09.xls
1628	UW3--4-5-Al-0(48)-5-3--10.xls
1639	UW3--4-5-Al-0(48)-5-3--11.xls

REFERENCES

1 Alekseev, A. G.; Barlas, R. A.; Tsidelko, T. I.; Shapoval, A. F.,
Effect of Particle Size on the Combustibility and Explosion Parameters of Dispersed Aluminum and Magnesium Powders, Editor: Nedin, V. V. In *Preduprezhdenie Vnezapnykh Vzryvov Gazodispersnykh Sist*, 66-73, (1971).

2 Assovskiy, I.G., Zhigalina, O.M., Kolesnikov-Svinarev, V.I.,
Gravity Effect in Aluminum Droplet Ignition and Combustion, *Fifth International Microgravvity Combustion Workshop*, Clevelend, OH, May 18-20, (1999).

3 Belyaev A.F., Frolov, Yu. V., Korotkov, A.I,
Combustion and Ignition of Particles of Finely Dispersed Aluminum, *Fizika Goreniya i Vzryva*, 4: 323-329, (1968).

4 Brossard, C., Ulas, A., Yen, C.L., and Kuo, K.K.,
Ignition and Combustion of Isolated Aluminum Particles in the Post-Flame Region of a Flat-Flame Burner, *16th International Colloquium on the Dynamic of Explosions and Reactive Systems*, Krakow, Poland, Aug 3-8, (1997).

5 Derevyga, M.E., Stesik, L.N., Fedorin,
E.A., Study of the Ignition and Combustion of Aluminum and Zinc in Air, *Fizika Goreniya i Vzyva*, 13: 852-857, (1977).

6 Ermakov, V. A.; Razdobreev, A. A.; Skorik, A. I.;
Pozdeev, V. V.; Smolyakov, S. S., Temperature of Aluminum Particles at the Moments of Ignition and Combustion, *Fizika Goreniya i Vzryva*, 18: 141-143, (1982).

7 Friedman, R., Macek, A.,
Ignition and Combustion of Aluminum Particles in Hot, Ambient Gases, *Combustion and Flame*, 6: 9-19, (1962).

8 Johnson C., Parr T., Hanson-Parr D., Hollins R., Fallis S., Higa K., Combustion and Oxidation of Metal Nanoparticles and Composite Particles, *Proceedings of 37-th JANNAF Combustion Subcommittee Meeting*, November 2000, 539-551, (2000).

9 Merzhanov, A.G., Grigorjev, Yu. M., Galchenko, Yu, A., Aluminum Ignition, *Combustion and Flame*, 29: 1-14, (1977).

10 Yuasa, S., Zhu Y., Sogo, S., Ignition and Combustion of Aluminum in Oxygen/Nitrogen Mixture Streams, *Combustion and Flame*, 108: 387-396, (1997).

11 Zhu, Y., Yuasa, Y., Effect of Oxygen Concentration on Combustion of Aluminum in Oxygen/Nitrogen Mixture Streams, *Combustion and Flame*, 115: 327-334, (1998).

12 M. A. Trunov and E.L. Dreizin, Ignition of Metastable Metal Based High Energy Density Fuels, *Ninth International Workshop on Combustion and Propulsion,* Villa arigola,19032 Lerici, La Spezia, Italy10-13 June 2003.

13 Mantell, L., Charles (1968) *Carbon and Graphite Handbook* New York, USA, Interscience Publishers.

14 Holman, J.P., (2002), *Heat Transfer* NY, McGraw-Hill.

15 Lide, D. R., & Frederikse, H. P. R. (1994-95). *CRC Handbook of Chemistry and Physics,* CRC Press.

16 Michael A. Trunov, Mirko Schoenitz, and Edward L. Dreizin, Ignition of Al-Mg Mechanical Alloys, Combustion Institute, Fall Eastern State Meeting.